Chemical Science

ROYAL SOCIETY OF CHEMISTRY

EDGE ARTICLE

View Article Online
View Journal | View Issue

Cite this: *Chem. Sci.*, 2024, **15**, 4824

All publication charges for this article have been paid for by the Royal Society of Chemistry

Received 18th December 2023
Accepted 13th February 2024

DOI: 10.1039/d3sc06816a

rsc.li/chemical-science

A reversible photoelectrochemical microsensor for dynamically monitoring sulfur dioxide in the epileptic brain†

Danying Lin,[a] Tao Lu,[b] Xiao Wang,[a] Xiaoxue Ye*[b] and Zhihong Liu *[ab]

Epilepsy is considered one of the most prevalent neurological disorders, yet the precise mechanisms underlying its pathogenesis remain inadequately elucidated. Emerging evidence implicates endogenous sulfur dioxide (SO_2) in the brain as playing a significant role in epilepsy and associated neuronal apoptosis. Consequently, tracking the dynamic fluctuations in the levels of SO_2 and its derivatives (SO_3^{2-}/HSO_3^-) provides valuable insights into the molecular mechanisms underlying epilepsy, with potential implications for its diagnosis and therapeutic intervention. Nonetheless, the absence of reversible *in vivo* detection tools constitutes a formidable obstacle in the real-time monitoring of SO_2 dynamics in the brain. In response to this challenge, we propose a novel approach involving a photoelectrochemical (PEC) microsensor capable of reversibly detecting SO_2. This microsensor leverages a reversibly recognizing dye for SO_2 and upconversion nanoparticles as the modulator of the excitation source for the photoactive material, enabling modulation of the photocurrent by the target. The reversible output of PEC signals allows for the monitoring of SO_2 levels in real time in the brains of epileptic mice. This study reveals the patterns of SO_2 level changes during epilepsy and provides insights into the neuroprotective mechanism of exogenous SO_2.

Introduction

Epilepsy stands as one of the prevailing neurological disorders, afflicting approximately 70 million individuals worldwide and contributing to 0.7% of the global disease burden.[1] Recurrent seizures often lead to hippocampal damage, resulting in subsequent cognitive impairment.[2] Despite its prevalence, the mechanism underlying the pathogenesis of epilepsy remains inadequately understood. SO_2, as a pivotal neurochemical transmitter in the brain, can be internally synthesized from sulfur-containing amino acids. Variations in its concentrations have been linked to a spectrum of cerebral disorders.[3] Previous investigations have posited the involvement of the sulfur dioxide (SO_2)/aspartate aminotransferase (AAT) pathway in the genesis of epilepsy and associated cerebral injury.[4] An abnormal elevation of the levels of SO_2 and its derivatives (SO_3^{2-}/HSO_3^-) has been considered as a possible basis for apoptosis of hippocampal neurons in epilepsy. Additionally, research has also delineated that SO_2 exerts a protective effect against brain injury associated with epilepsy through various molecular mechanisms.[5] It is evidently imperative to monitor the levels of endogenous SO_2 in the brain to gain insights into the pathogenic mechanisms of this disorder.[6] Regrettably, the dearth of suitable *in situ* analysis tools has hindered our ability to track time-resolved fluctuations in SO_2 levels during epilepsy.

In vivo electrochemical analysis, utilizing implantable microelectrodes, represents a robust methodology for real-time monitoring of neurochemicals in the living brain, offering exceptional spatiotemporal resolution and sensitivity.[7] More recently, photoelectrochemical (PEC) sensing has emerged as a promising tool for *in vivo* analysis. Its design, predicated on the chemical recognition of a small molecule dye, has proved to be particularly adept at selectively detecting electrochemically inert neurochemicals, such as SO_2, which are difficult to detect directly through faradaic signals.[8] However, a major challenge associated with this method lies in monitoring dynamic changes in target levels over time, due to the fact that the vast majority of known recognition processes are irreversible, thereby only reflecting a monotonic increase in the target concentration. To date, only a limited number of conditional reversible dyes have been reported for sulfite detection, which typically necessitate the addition of sulfur dioxide scavengers or oxidants (*e.g.*, formaldehyde, hydrogen peroxide) to facilitate the reverse process.[9] Consequently, these reversible dyes fall short in dynamically monitoring sulfite in living organisms. Obviously, to achieve real-time monitoring of the fluctuating

[a]*College of Chemistry and Molecular Sciences, Wuhan University, Wuhan 430072, China. E-mail: zhhliu@whu.edu.cn*

[b]*College of Health Science and Engineering, Ministry of Education Key Laboratory for the Synthesis and Application of Organic Functional Molecules, Hubei University, Wuhan 430062, China. E-mail: yexxchem@hubu.edu.cn*

† Electronic supplementary information (ESI) available. See DOI: https://doi.org/10.1039/d3sc06816a

levels of SO_2 *in vivo*, the dye must be capable of swiftly and spontaneously undergoing a reversible reaction in response to both increasing and decreasing SO_2 concentrations without the need for additional reagents, including catalysts, oxidants or SO_2 scavengers. Unfortunately, as of now, there have been no reported instances of a reversible dye capable of meeting this formidable challenge.

In this work, we have successfully engineered a reversible photoelectrochemical (PEC) microsensor, employing a spontaneous reversible dye founded on the Michael addition reaction, to dynamically track the fluctuations in SO_2 levels in the brains of epileptic mice. Initially, three dyes were designed and synthesized to enable reversible recognition of SO_2. The effect of the electron cloud density of the recognition site on the reversibility of the dye was investigated. To accurately detect intracerebral SO_2 concentrations in the range of 5–25 μM, a dissociation constant (K_d) value of approximately 10 μM is required.[10] Eventually, we identified an optimized dye, boasting a desirable K_d value of 9.6 μM for detecting SO_2 in the brain. More importantly, the addition reaction between the dye and sulfur dioxide can occur spontaneously and reversibly. Afterwards, the selected dye underwent further modification by attachment to upconversion nanoparticles (UCNPs), thereby giving rise to a fluorescence resonance energy transfer (FRET)-based nanoprobe. This FRET-based nanoprobe was subsequently co-modified with photoactive materials on Ti wires to construct a reversible PEC microsensor. Specifically, the FRET process led to the quenching of upconversion luminescence (UCL) which functioned as the excitation source of the photoactive materials, resulting in a low photocurrent of the PEC sensor. The introduction of SO_2 caused a reduction in FRET efficiency, thereby increasing both the UCL and photocurrent. The reversible nature of the nanoprobe allowed it to spontaneously form a free state as SO_2 levels decreased, again leading to a reduced PEC signal (Scheme 1). The proposed microsensor showed excellent reversible response both *in vitro* and *in vivo*, and successfully monitored SO_2 in three brain regions of epileptic mice, revealing the law of SO_2 fluctuations and providing insights into the neuroprotective mechanism of exogenous SO_2.

Results and discussion

Design and response of the reversible molecular recognizers

We employed the concept of the Michael addition reaction, which involves the conjugated addition between an electrophilic conjugated system and a nucleophilic electron donor, to design reversibly recognizing dyes for SO_2. The reversibility and sensitivity of the dyes, represented by K_d, can be adjusted by modifying the molecular structure to manipulate the electron density. Herein, we rationally designed and synthesized three novel SO_2 reversible dyes named rSO_2-1, rSO_2-2, and rSO_2-3, respectively (Scheme 2). The benzopyran unit was selected as the recognition site, and three different electron donors including *p*-phenylenediamine, *p*-phenylamine, and *p*-phenylacetamido were introduced to adjust the charge density of the recognition site, thus endowing the molecules with flexible reversible properties. The successful synthesis of rSO_2 dyes was confirmed by ^{1}H NMR, ^{13}C NMR and HRMS (Fig. S1–S9†). To verify the reaction mechanism of rSO_2 toward SO_2, specifically taking rSO_2-2 as the representative, the reaction products were characterized by mass spectrometry and ^{1}H NMR. The observed peak at *m*/*z* 397.1249 $[M + Na]^+$ in the mass spectrum indicated the molecular weight to be 374, corresponding to the formula $C_{19}H_{22}N_2O_4S$, as expected. Changes in the chemical shift calculated in the ^{1}H NMR spectrum suggested a structural

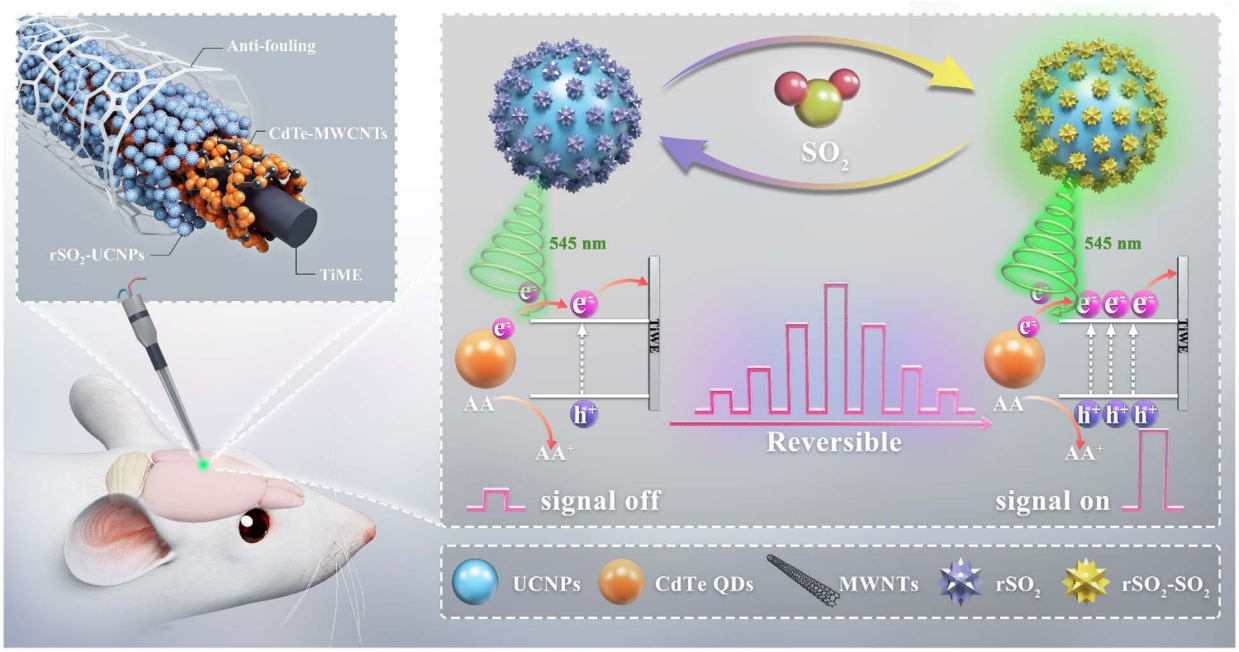

Scheme 1 Schematic illustration of the response mechanism of the PEC microsensor for reversible sensing of SO_2.

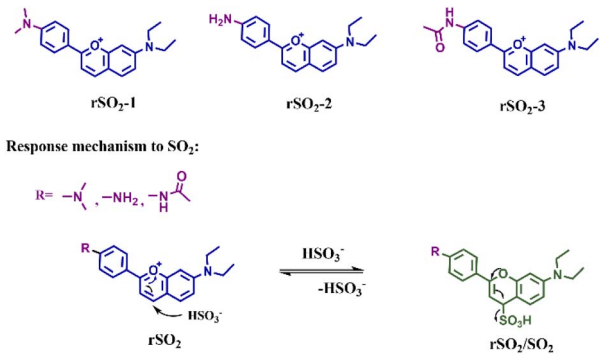

Scheme 2 The molecular structures of rSO_2-1, rSO_2-2, and rSO_2-3, as well as the response mechanism of rSO_2.

alteration in rSO_2-2. The obtained results support the proposed mechanism outlined in Scheme 2. Fig. 1a illustrates the absorption spectra of rSO_2-1, rSO_2-2, and rSO_2-3, showing a sequential blue-shift. This shift is consistent with the decreasing electron-donating ability of dimethylamino, amino, and acetamido connected to the conjugated system. Consequently, the electrophilic abilities of the recognition sites were enhanced due to the higher charge densities (0.02627, 0.03019, and 0.03349, as calculated by the extended Huckel method) (Fig. 1b). Since SO_2 exists in the form of HSO_3^- and SO_3^{2-} (1 : 3, M/M) in organisms, SO_3^{2-} was used for *in vitro* experiments. To evaluate the reversibility of rSO_2 dyes, dilution experiments were carried out. Results from the 10-fold dilution indicate a rapid and reversible response of rSO_2-1 (Fig. 1c), as well as rSO_2-2 (Fig. 1d), which is predominantly dependent on the dose of SO_2. rSO_2-3 (Fig. 1e) exhibited poor dose-dependent reversibility, possibly due to the strong cohesion caused by the weak electron-donating ability of the acetylamino group. These dyes demonstrated exceptional selectivity towards SO_2, without any interference from ROS, H_2S, 40 μM GSH and other biothiols, whereas a high concentration of GSH (10 mM) noticeably affected their selectivity (Fig. S11†). These findings indicate the potential use of these dyes for detecting SO_2 in the intercellular fluid, as the low concentration of GSH in this fluid does not compromise the selectivity of the dye.[11] However, it is not suitable for detecting intracellular SO_2 due to the substantial influence of the high concentration of GSH within the intracellular environment.[12] Fig. 1f and g depict the gradual decrease in absorption of rSO_2-1 and rSO_2-2 as the concentration of SO_2 increased. Additionally, the widely used mercaptan scavenger *N*-methylmaleimide (NMM) was used to explore the reversibility of the reaction. Upon NMM being added to the dye solutions pretreated with SO_2, the UV-Vis absorption was restored to varying degrees since SO_2 was removed (Fig. 1h and i). The calculated K_d values for rSO_2-1 and rSO_2-2, based on the slope of

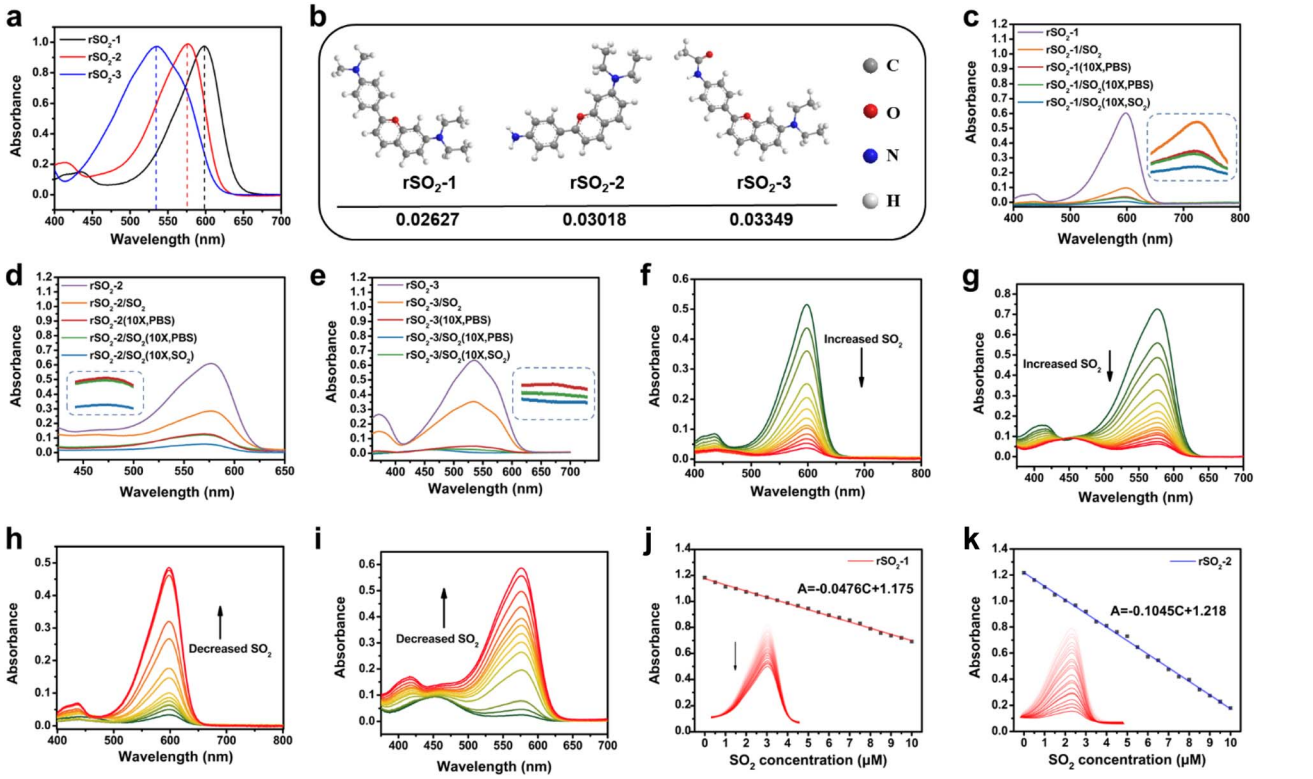

Fig. 1 (a) Absorption spectra of rSO_2-1, rSO_2-2, and rSO_2-3. (b) Charge density at the recognition site of rSO_2-1, rSO_2-2, and rSO_2-3 calculated by the extended Huckel method. (c–e) The initial mixtures of SO_2 and rSO_2-1 (rSO_2-1/SO_2) (c), rSO_2-2 (rSO_2-2/SO_2) (d), and rSO_2-3 (rSO_2-3/SO_2) (e) were diluted 10-fold into the PBS containing no or 10 μM SO_2. (f and g) UV-vis response of rSO_2-1 (f) and rSO_2-2 (g) upon addition of SO_2 (0–200 μM SO_2 in rSO_2-1 and 0–100 μM SO_2 in rSO_2-2). (h and i) Reversible changes in the absorption spectra of rSO_2-1/SO_2 (h) and rSO_2-2/SO_2 (i) upon addition of NMM (0–1 mM). (j and k) Absorbance of rSO_2-1 (j) and rSO_2-2 (k) as a function of SO_2 concentration (0–20 μM).

the absorbance-concentration line, were 21.3 μM and 9.6 μM, respectively (Fig. 1j and k). Considering the physiological level of SO_2 in the cerebrospinal fluid (CSF) (within the range of 5–25 μM),[10] rSO_2-2 is more suitable for the reversible analysis of SO_2 in the brain.

Properties of the rSO_2-UCNPs nanoprobe

Furthermore, PAA-modified $NaYF_4$:Yb,Er UCNPs were synthesized with the intention of constructing a FRET-based nanoprobe in combination with rSO_2-2. Transmission electron microscopy (TEM) images revealed that the UCNPs exhibited a uniform size distribution, with an average diameter of about 37 nm (Fig. S12†). X-ray diffraction (XRD) patterns confirmed that the obtained nanoparticles possessed a hexagonal phase (Fig. S13†). Importantly, the absorption band of rSO_2-2 fits nicely with the emission band of UCNPs at 545 nm, facilitating efficient energy transfer from UCNPs to rSO_2-2 and UCL quenching (Fig. 2a). FRET occurred between UCNPs and rSO_2-2 when the positively charged rSO_2-2 assembled on the surface of the negatively charged UCNPs *via* electrostatic interaction. The zeta potential shifted from −30 mV for bare UCNPs to −20 mV for rSO_2-UCNPs, indicating the binding of rSO_2-2 to UCNPs (Fig. S14†). As anticipated, the degree of fluorescence quenching increased with the loading of rSO_2-2, reaching a maximum quenching efficiency of 95% with a dose of 100 μM rSO_2-2 (Fig. 2b). In the presence of SO_2, FRET was inhibited, leading to the recovery of UCL intensity (Fig. 2c). Subsequent addition of NMM removed sulfite from the solution, resulting in dissociation of sulfite from the adducts, accompanied by the reoccurrence of FRET and UCL quenching (Fig. 2d). The above results implied that rSO_2-UCNPs exhibited a reversible response to sulfite, with significant changes in the UCL intensity of UCNPs at 545 nm, which can be exploited to modulate the photocurrent signal.

Characteristics of the PEC microsensor

A 70 μm-diameter titanium wire was packaged in a glass capillary with the exposed length at 600 μm (denoted as TiME, Fig. S15†), which served as the working electrode. To improve the measurement depth *in vivo*, a 200 μm optical fiber was inserted into the front end of the drawn glass capillary tube and encapsulated with optical glue (Fig. 2e). This configuration

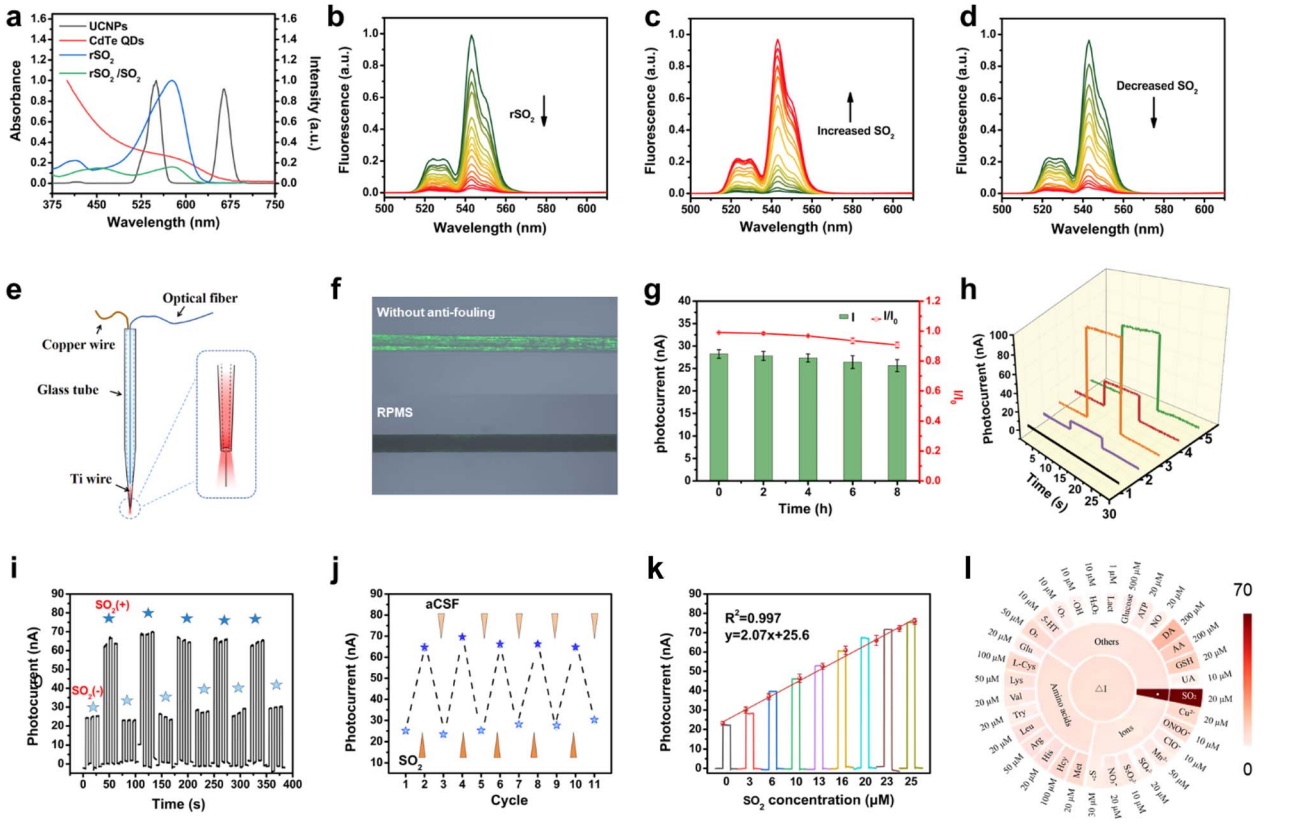

Fig. 2 (a) Normalized fluorescence spectrum of UCNPs excited at 980 nm and the absorption spectra of rSO_2 and CdTe QDs. (b and c) Fluorescence spectra of rSO_2-UCNPs upon addition of different amounts of rSO_2 (b) and SO_2 (c). (d) Fluorescence spectra of rSO_2-UCNPs with the removal of SO_2. (e) Schematic illustration of the architecture of designed microelectrode TiME. (f) Fluorescence images of microelectrodes with different coatings after adsorption of FITC-BSA (1%) for 8 h: rSO_2-UCNPs/CdTe-MWCNTs/TiME (top) and rSO_2-UCNPs/CdTe-MWCNTs/BSA-GA/TiME (bottom). (g) Photocurrent signals obtained at RPMS in aCSF containing 1% BSA. (h) Photocurrent of bare and modified microelectrodes excited at 980 nm in aCSF: (1) TiWE, (2) CdTe-MWNTs/TiME, (3) UCNPs/CdTe-MWNTs/TiME, and rSO_2-UCNPs/CdTe-MWNTs/TiME before (4) and after (5) incubation with 20 μM SO_2. (i) Reversible cycles observed in the PEC response of RPMS in aCSF without or with 20 μM SO_2. (j) Photocurrent obtained from the reversible cycles described in (i). (k) Photocurrent response of RPMS in aCSF toward varying concentrations of SO_2. (l) Selectivity test of SO_2 with interfering substances.

allowed stable transfer of the light *via* the optical fiber and optical glue, enabling *in situ* excitation and detection of deep brain regions. Then, photoactive materials composed of CdTe QDs and acidified multiwall carbon nanotubes (CdTe-MWNTs) were prepared (Fig. S16–S18†), and modified on the tip of TiME through titanium–carboxyl interaction.[13] The resulting microphotoelectrode was referred to as CdTe-MWNTs/TiME for generating photocurrent. Next, the rSO_2-UCNPs nanoprobe was assembled on the surface of CdTe-MWNTs/TiME by immersion and drying to fabricate the reversible PEC sensing platform (rSO_2-UCNPs/CdTe-MWNTs/TiME). It is worth noting that biofouling of implanted microelectrodes can negatively impact their sensing performance by causing passivation. To address this issue, an anti-biofouling modification was applied. Specifically, a three-dimensional bovine serum albumin-glutaraldehyde (BSA-GA) film was introduced to enhance the anti-fouling properties of the microelectrode, and the entire reversible PEC microsensor was obtained (referred to as RPMS).[14] The hydrophilicity of the modified surface was confirmed through contact angle tests (Fig. S19†). Additionally, protein adsorption tests were carried out, demonstrating that the BSA-GA coating significantly reduced protein adsorption (Fig. 2f). After immersing in a BSA solution for 8 hours, the photocurrent response of RPMS remained at 91.9% of its initial response (Fig. 2g), indicating the effectiveness of the anti-fouling modification. Scanning electron microscopy (SEM) (Fig. S20†) confirmed the step-by-step modification process and revealed the distribution of Cd, Te, Na, Y, F, Yb, Er, O, C, N, and S on the surface of RPMS, indicating the successful modification of TiME. Then, the PEC performance of the aforementioned RPMS was characterized to validate the capability of the rSO_2-UCNPs nanoprobe as an excitation source to trigger CdTe-MWNTs to generate photocurrent signals and its response to sulfite. As depicted in Fig. 2h, a minimal photocurrent response of 8 nA (curve 2) was observed for CdTe-MWNTs/TiME under 980 nm light irradiation, as CdTe-MWNTs have limited absorption in the NIR light range. In contrast, the as-prepared UCNPs/CdTe-MWNTs/TiME showed the largest photocurrent response of 90 nA (curve 3), due to the effectively excited CdTe-MWNTs by the UCL of UCNPs at 545 nm. After that, the introduction of rSO_2 quenched the UCL, resulting in a 65% drop in photocurrent compared to the UCNPs/CdTe-MWNTs/TiME (curve 4). Finally, the incubation of sulfite at a concentration of 20 μM resulted in a sharp increase in photocurrent (curve 5) as the FRET process was inhibited, leading to the recovery of UCL and an increase in the photocurrent signal. Control experiments were conducted by treating UCNPs/CdTe-MWNTs/TiME in artificial cerebrospinal fluid (aCSF) with and without 50 μM sulfite, respectively, to exclude the influence of sulfite on other electrode modification materials (Fig. S21†). These results validated the principle and effectiveness of our sensing strategy.

Reversible response and analytical performance of the microsensor towards SO_2

The reversibility of the microsensor RPMS was evaluated to assess its ability for real-time monitoring of dynamic fluctuations in SO_2 levels. Fig. 2i and j show the reversibility analysis by incubating the RPMS in SO_2-free aCSF and aCSF containing 20 μM SO_2. It was observed that the photocurrent response sharply increased when the RPMS was incubated with aCSF containing SO_2, while a decreased response was observed with SO_2-free aCSF. Additionally, the reversibility of the RPMS was maintained after 5 cycles, indicating its robust performance. Under optimal conditions (Fig. S22†), the reversibility of RPMS was further explored (Fig. S23†). As expected, the PEC signal gradually enhanced with the addition of SO_2, and a gradual drop in the PEC signal was observed upon stepwise dilution of the SO_2 solution with aCSF. Moreover, a linear correlation between the photocurrent and SO_2 concentration in the range of 3–25 μM was established, with a detection limit of 0.14 μM, ensuring quantitative detection (Fig. 2k). The fast response of 120 s for recognition and 150 s for the reversible process enabled real-time and dynamic monitoring of SO_2 levels (Fig. S24†). Benefiting from the high selectivity of rSO_2, the excellent specificity for SO_2 was demonstrated by co-incubating the RPMS with various coexisting species in the biosystem (Fig. 2l). Ascorbic acid (AA), a common electron donor in the biosystem with a low redox potential, has the potential to affect the anode photocurrent through redox reactions.[15] Although the photocurrent can be affected by low AA levels, negligible effect was found when AA reached over 100 μM (Fig. S25†). Considering the physiological levels of AA (200 ± 50 μM), aCSF with 200 μM AA was used in *in vitro* experiments. RPMS also showed good photostability after continuous off-on-off irradiation (Fig. S26 and S27†), as well as good reproducibility for independent electrodes (Fig. S28†).

Reversible monitoring of SO_2 in the brain

As demonstrated above, the developed RPMS exhibited satisfactory reversible properties, as well as remarkable analytical performance, providing a reliable *in vivo* analysis platform for dynamic monitoring of SO_2 in the brain of living animals. Before the *in vivo* application, toxicity of RPMS was assessed by evaluating the cytotoxicity of the electrode modification material. HBMEC cells were incubated in dishes coated with CdTe-MWCNTs/rSO_2-UCNPs/BSA-GA film for 48 h. Subsequently, cell viability was determined through co-staining with calcein AM-propidium iodide. The utilization of confocal microscope imaging demonstrated favorable cell growth on the surface coated with CdTe-MWCNTs/rSO_2-UCNPs/BSA-GA (Fig. S29†), thus indicating good biocompatibility of the materials.

Furthermore, the standard deviation of RPMS in five repeated measurements was less than 5% (Fig. S30†). These results further confirm the excellent performance of the RPMS for *in vivo* detection.

In the first instance, RPMS was used to detect exogenous SO_2 in living mouse brain. The mice received *in situ* injection of Na_2SO_3 in the hippocampus (CA1) followed by the scavenger NMM. PEC signals were recorded after each injection. As depicted in Fig. 3a and b, a significantly elevated PEC signal following the *in situ* injection of Na_2SO_3 was observed, indicating a robust response towards SO_2 *in vivo*. Subsequently,

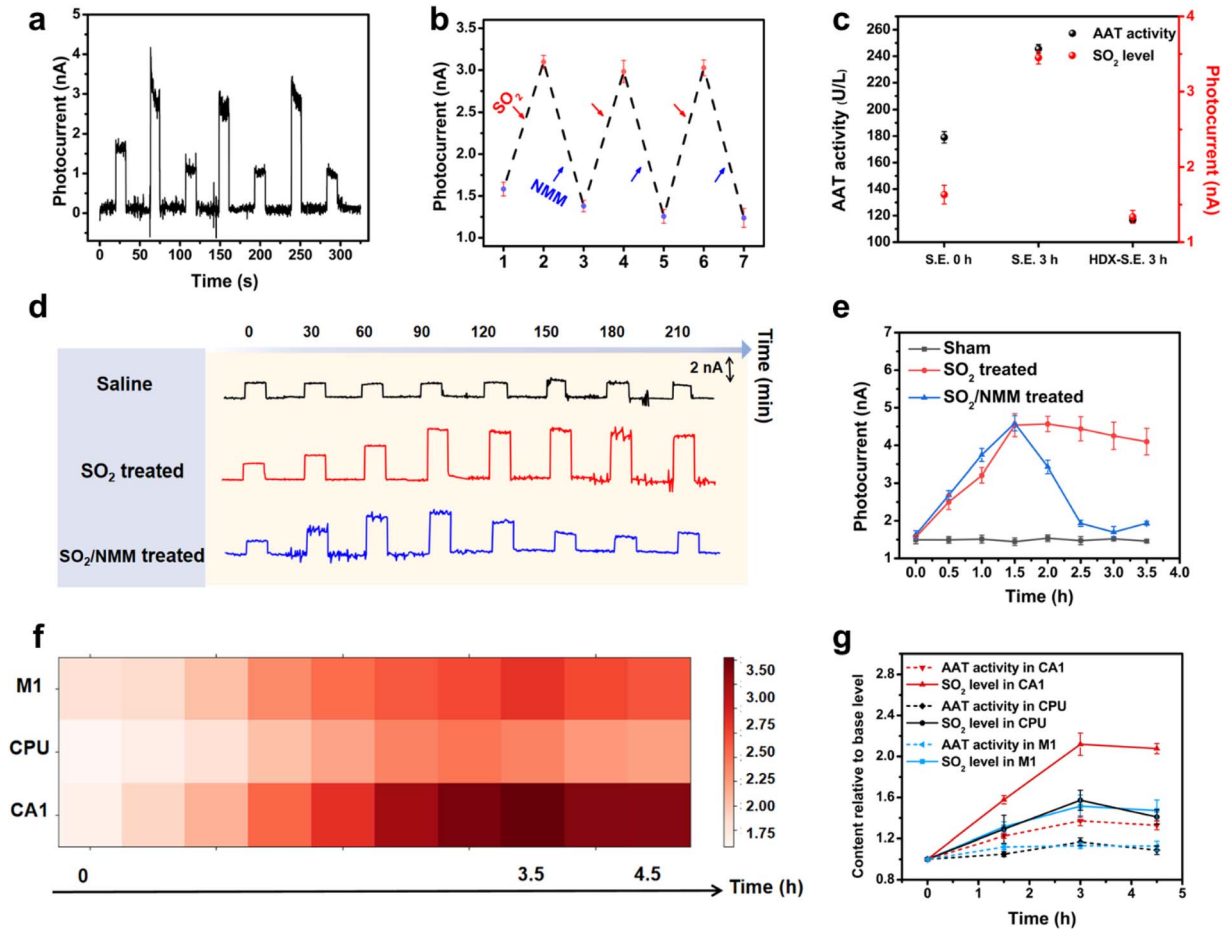

Fig. 3 (a) Reversible photocurrent responses recorded at RPMS in CA1 of a live mouse brain following local microinjections (1 μL min^{-1} for 60 s) of Na_2SO_3 and NMM in a continuous manner. (b) Photocurrents obtained from the reversible responses described in (a). (c) SO_2 levels (red) and AAT activity (black) in the hippocampus of epileptic mice pretreated with HDX. (d) Time-dependent PEC signals obtained with RPMS in CA1 of acute SO_2 poisoning mice. (e) Photocurrents obtained from (d). (f) Matrix map of photocurrents in the CA1, M1 and CPU regions of epileptic mice. (g) Analysis of SO_2 levels and AAT activity in the CA1, M1 and CPU regions of epileptic mice.

NMM was injected to eliminate SO_2, resulting in a noticeably attenuated PEC signal. The RPMS successfully recorded signals from three consecutive Na_2SO_3/NMM injections, and the photocurrent response varied in accordance with the levels of SO_2, demonstrating the excellent reversible detection capability of SO_2 *in vivo* by the RPMS.

Subsequently, the ability of RPMS to dynamically monitor SO_2 *in vivo* was further investigated in a mouse model of acute SO_2 poisoning. The mice were randomly divided into two groups: one group received injection of Na_2SO_3 as the SO_2 source, while the other group received saline as a control. As displayed in Fig. 3d and e, an intraperitoneal injection of Na_2SO_3 induced an elevated photocurrent response of RPMS implanted in CA1 over time, but no remarkable shift followed the injection of saline, suggesting that the increase in SO_2 level in the mouse brain was specifically caused by the rapid absorption of Na_2SO_3. In addition, the level of SO_2 in the brain reached its maximum at 1.5 h after poisoning and then slowly decreased. However, upon the injection of NMM, there was a dramatic decrease in photocurrent. The above results again validated the capability of RPMS to dynamically monitor and track real-time changes of SO_2 levels *in vivo*.

Tracking the SO_2 level in the brain of epileptic mice

Epilepsy is a neurological disorder accompanied by abnormal discharges, and can cause irreversible damage to the brain. While previous studies have indicated the involvement of endogenous SO_2 in epilepsy and associated neuronal apoptosis,[5,16] limited research tools impeded the investigation of the dynamics of SO_2 fluctuations in the brain throughout the course of epilepsy. In the present study, we aimed to investigate the real-time changes in endogenous SO_2 levels in the extracellular fluid of the living brain during epilepsy. Firstly, the kainic acid (KA)-induced status epilepticus (S.E.) model was established according to the existing literature.[17] Then, RPMS was utilized to monitor intercellular SO_2 levels in different brain regions including M1, CPU and CA1 (Fig. 3f, S31†). The results revealed a gradual increase in SO_2 levels in all three brain regions after epilepsy, with the highest levels at approximately 3 h. SO_2 levels in the CPU region reach their peak slightly earlier

than those in the CA1 and M1 regions. The photocurrent response in M1, CPU and CA1 rose to 151%, 158% and 216%, respectively. Notably, CA1 exhibited the highest magnitude of photocurrent rise compared to M1 and CPU during S.E., indicating that CA1 was the most affected brain region. Moreover, the CA1 region demonstrates the most rapid elevation rate, while the elevation rates of SO_2 levels in the CPU and M1 regions are comparable but slower (Fig. S32†). The above results suggested that during epilepsy, the SO_2 levels in different brain regions undergo a significant increase to varying degrees with CA1 being the most prominently affected and underscored the heterogeneity in endogenous SO_2 alterations across distinct cerebral regions during epilepsy.

As an endogenous gaseous molecule, SO_2 can be endogenously generated from sulfur-containing amino acids by an AAT dependent pathway.[18] To gain further insight into the AAT/SO_2 pathway in epilepsy, we determined AAT activity in three brain regions (CA1, M1 and CPU). As can be seen from Fig. 3g, the variation trend of AAT activity was in harmony with that of SO_2 levels. It was reasonable to predict that the increased SO_2 production is preceded by an upregulation of AAT activity. To validate this hypothesis, a second group of mice was pretreated with AAT inhibitor L-aspartate-hydroxamate (HDX). As expected, the inhibition of AAT activity led to a significant decrease in both the SO_2 levels and AAT activity in CA1 (Fig. 3c). These findings provide further evidence that the upregulation in AAT activity in epilepsy is one of the major factors contributing to the increase of SO_2 content in the brain of epileptic mice. The results support the involvement of the AAT/SO_2 pathway in epileptic processes and highlight the potential significance of AAT as a target for therapeutic interventions aimed at modulating SO_2 levels in epilepsy.

Neuroprotective mechanism of exogenous sulfur dioxide

Low-concentration SO_2 pretreatment has been reported to have a neuroprotective effect against neurological injuries.[5] In investigating this neuroprotective effect and related mechanism in the context of epilepsy for the first time, mice were subjected to an experiment involving the administration of a low concentration of SO_2 (25 μmol kg^{-1}) 30 minutes prior to KA injection. TUNEL and HE staining were performed to evaluate the neuronal injury in the hippocampus. Fig. 4a and b depict that, in contrast to the S.E. group, the SO_2-pretreated S.E. group exhibited comparatively minor neuronal damage, indicating the protective efficacy of SO_2 pretreatment against epilepsy-induced neuronal injury. Furthermore, the inhibition of AAT by HDX exacerbated epilepsy-induced neuronal injury, underscoring the crucial role of SO_2 in neuronal protection from such injuries. To delve further into the neuroprotective mechanism, the recording of SO_2 levels in the CA1 region of the hippocampus was conducted using RPMS. The results demonstrated a swift increase in the SO_2 level following SO_2 pretreatment, as illustrated in Fig. 4c and S33.† Subsequent to KA-induced epilepsy

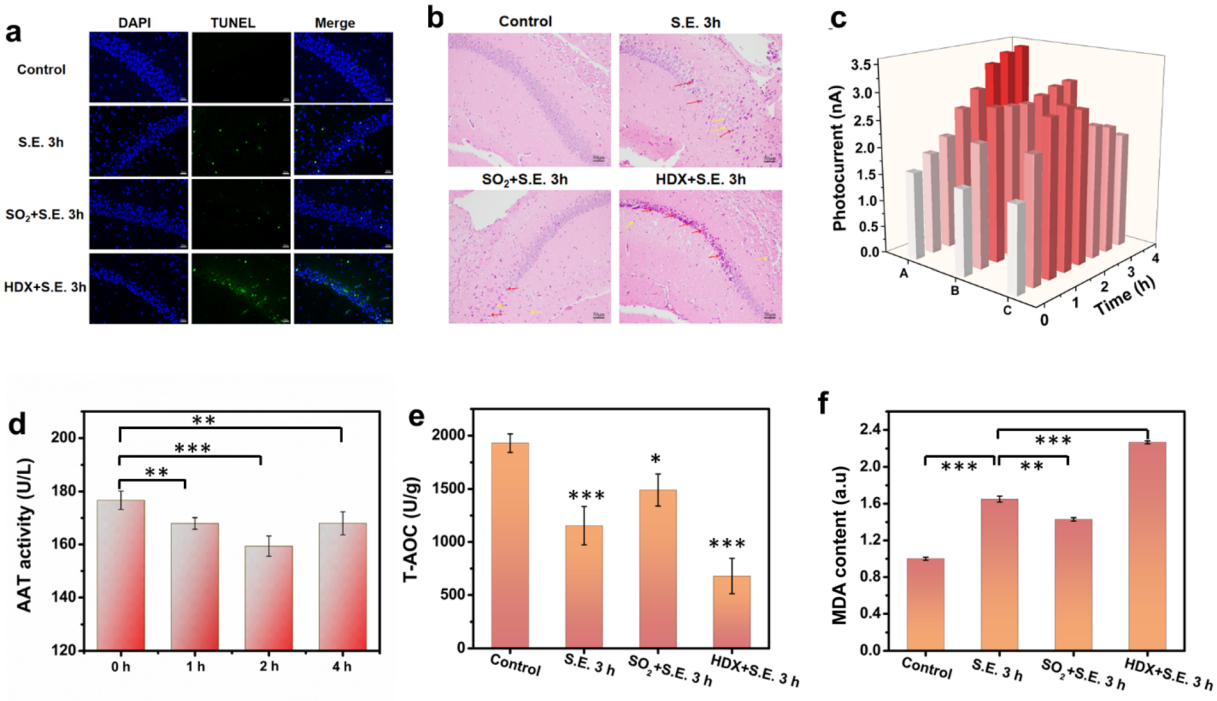

Fig. 4 (a) TUNEL staining of CA1 in the mice with seizures for 3 h pretreated with SO_2 and HDX. (b) HE staining of CA1 in the mice with seizures for 3 h pretreated with SO_2 and HDX. Yellow arrows represent inflammatory cells, red arrows represent necrotic neurons. (c) Time-dependent photocurrents obtained using RPMS in the CA1 region with different treatments: KA-induced epilepsy (S.E.) and KA-induced epilepsy with the pretreatment of SO_2 (25 μmol kg^{-1}) (SO_2 + S.E.). (d) AAT activity in the hippocampus of epileptic mice pretreated with SO_2 at different time points (*p < 0.05, **p < 0.01, and ***p < 0.001). (e) Total antioxidant capacity (T-AOC) in the hippocampus of the mice with seizures for 3 h pretreated with SO_2 and HDX. (f) MDA content in the hippocampus of the mice with seizures for 3 h pretreated with SO_2 and HDX.

induction, the SO_2 level continued to increase, albeit with reduced magnitude compared to the S.E. group. Throughout the recording duration, the average sulfur dioxide concentration was higher than that of the control group but lower than that of the S.E. group. To explore the underlying cause of this disparity, we measured AAT activity in the hippocampus at different time points (Fig. 4d). The outcomes revealed an inhibition of AAT activity post SO_2 pretreatment, with the lowest levels of activity being observed after 2 hours and progressively recovering afterwards. These findings suggest that the restrained increase in SO_2 levels in SO_2-pretreated epileptic brains can be attributed to the inhibition of AAT activity by exogenous SO_2.

However, the question arises as to what may be the mechanisms for this neuroprotective effect of low SO_2 pretreatment. Oxidative stress is one of the primary mechanisms implicated in S.E.-induced neuronal damage.[5] Sulfur dioxide pretreatment has been found to enhance antioxidant capacity during myocardial ischemia.[19] Therefore, we hypothesize that the neuroprotective mechanism of SO_2 pretreatment in epilepsy may be associated with its augmentation of antioxidant capacity. To verify this hypothesis, we examined the total antioxidant capacity (T-AOC) (Fig. 4e) and MDA (a biomarker for oxidative stress) (Fig. 4f) levels in the brains of different mouse groups. The results revealed a correlation between the degree of neuronal damage and oxidative stress, indicating that oxidative stress is a major contributing factor in the model of neuronal damage induced by epilepsy. More importantly, the antioxidant capacity of the epilepsy group pretreated with SO_2 significantly improved, while the HDX group exhibited the lowest antioxidant capacity, aligning with the findings from TUNEL and HE staining. These results underscore the pivotal role of SO_2 in protecting against brain injury induced by epilepsy, highlighting that low concentrations of SO_2 pretreatment contribute to a neuroprotective effect by upregulating antioxidant capacity in the brain.

Conclusions

The developed reversible PEC microsensor (RPMS) based on a FRET-modulated signal has demonstrated its effectiveness for dynamic monitoring of SO_2 levels in the living mouse brain. The utilization of the Michael addition reaction between rSO_2 and SO_2 enables reversible detection and ensures high selectivity of RPMS. The biocompatibility of the microsensor has been confirmed, and it has exhibited excellent analytical performance both *in vitro* and *in vivo*, making it suitable for real-time monitoring in living brains. By utilizing this microsensor, the study effectively demonstrated the variation of endogenous SO_2 in distinct cerebral regions during epilepsy, along with elucidating the neuroprotective mechanism of low concentration exogenous SO_2 in mitigating neuronal damage induced by epilepsy. This work introduces a novel tool for recording SO_2 fluctuations in living brains, which has the potential to contribute to the understanding of molecular-level mechanisms of brain function and the development of treatments for various neurological disorders.

Author contributions

D. Lin: most of the experiments and writing of the manuscript. T. Lu and X. Wang: *in vivo* experiments. X. Ye: supervision of experiments, discussion, and writing of the manuscript. Z. Liu: writing, review, and editing of the manuscript, funding acquisition and supervision.

Conflicts of interest

There are no conflicts to declare.

Acknowledgements

The authors acknowledge the financial support from the National Natural Science Foundation of China (Grant No. 22276047, 22227804). All animal studies were performed according to the Guidelines for the Care and Use of Laboratory Animals of the Chinese Animal Welfare Committee and approved by the Institutional Animal Care and Use Committee, Wuhan University Center for Animal Experiment, Wuhan, China.

References

1 G. K. Mbizvo, K. Bennett, C. R. Simpson, S. E. Duncan and R. F. M. Chin, *Epilepsy Res.*, 2019, **157**, 106192.
2 (*a*) Y. Xiong, H. Zhou and L. Zhang, *Brain Res.*, 2014, **1557**, 190–200; (*b*) U. Sayin, T. P. Sutula and C. E. Stafstrom, *Epilepsia*, 2004, **45**, 1539–1548.
3 H. Yan, Y. Wang, F. Huo and C. Yin, *J. Am. Chem. Soc.*, 2023, **145**, 3229–3237.
4 M. Niu, Y. Han, Q. Li and J. Zhang, *Neurosci. Lett.*, 2018, **665**, 22–28.
5 Y. Han, W. Yi, J. Qin, Y. Zhao, J. Zhang and X. Chang, *Neurosci. Lett.*, 2014, **563**, 149–154.
6 W. Zhang, F. Huo, Y. Yue, Y. Zhang, J. Chao, F. Cheng and C. Yin, *J. Am. Chem. Soc.*, 2020, **142**, 3262–3268.
7 (*a*) Y. Wang, Y. Qian, L. Zhang, Z. Zhang, S. Chen, J. Liu, X. He and Y. Tian, *J. Am. Chem. Soc.*, 2023, **145**, 2118–2126; (*b*) F. Zhu, Y. Xue, W. Ji, X. Li, W. Ma, P. Yu, Y. Jiang and L. Mao, *Angew. Chem., Int. Ed.*, 2023, **62**, e2022124; (*c*) C. Yang, Q. Cao, P. Puthongkham, S. T. Lee, M. Ganesana, N. V. Lavrik and B. J. Venton, *Angew. Chem., Int. Ed.*, 2018, **57**, 14255–14259; (*d*) X. He and A. G. Ewing, *J. Am. Chem. Soc.*, 2022, **144**, 4310–4314; (*e*) E. F. Megan and R. M. Wightman, *Pharmacol. Rev.*, 2017, **69**, 12; (*f*) C. Wang, X. Bi, X. Zhao, M. Zhou, Y. Ding and Y. Lin, *ACS Sustain. Chem. Eng.*, 2019, **7**, 3715–3721; (*g*) A. Meiller, E. Sequeira and S. Marinesco, *Anal. Chem.*, 2020, **92**, 1804–1810; (*h*) K. Zhang, H. Wei, T. Xiong, Y. Jiang, W. Ma, F. Wu, P. Yu and L. Mao, *Chem. Sci.*, 2021, **12**, 7369–7376.
8 X. Ye, X. Wang, Y. Kong, M. Dai, D. Han and Z. Liu, *Angew. Chem., Int. Ed.*, 2021, **60**, 11774–11778.
9 (*a*) H. Zhu, X. Zhang, C. Liu, Y. Zhang, M. Su, X. Rong, X. Wang, M. Liu, X. Zhang and W. Sheng, *Sens. Actuators, B*, 2022, **366**, 131962; (*b*) Y. Zhang, L. Guan, H. Yu, Y. Yan,

L. Du, Y. Liu, M. Sun, D. Huang and S. Wang, *Anal. Chem.*, 2016, **88**, 4426–4431.
10 Y. Kimura, N. Shibuya and H. Kimura, *Br. J. Pharmacol.*, 2019, **176**, 571–582.
11 (*a*) M. Węgrzynowicz, W. Hilgier, A. Dybel, S. S. Oja, P. Saransaari and J. Albrecht, *Neurochem. Int.*, 2007, **50**, 883–889; (*b*) K. Q. Do, A. Trabesinger, H. M. Kirsten-Krüger, C. J. Lauer, U. Dydak, D. Hell, F. Holsboer, P. Boesiger and M. Cuénod, *Eur. J. Neurosci.*, 2000, **12**, 3721–3728.
12 (*a*) Z. Liu, X. Zhou, Y. Miao, Y. Hu, N. Kwon, X. Wu and J. Yoon, *Angew. Chem., Int. Ed.*, 2017, **56**, 5812–5816; (*b*) K. Aoyama, *Int. J. Mol. Sci.*, 2021, **22**, 5010.
13 W. Wang, W. Feng, J. Du, W. Xue, L. Zhang, L. Zhao, Y. Li and X. Zhong, *Adv. Mater.*, 2018, **30**, 1705746.
14 J. Sabaté del Río, O. Y. F. Henry, P. Jolly and D. E. Ingber, *Nat. Nanotechnol.*, 2019, **14**, 1143–1149.
15 M. Zhang, K. Liu, L. Xiang, Y. Lin, L. Su and L. Mao, *Anal. Chem.*, 2007, **79**, 6559–6565.
16 A. Finegersh, C. Avedissian, S. Shamim, I. Dustin, P. M. Thompson and W. H. Theodore, *Epilepsia*, 2011, **52**, 689–697.
17 P. Vincent and C. Mulle, *Neuroscience*, 2009, **158**, 309–323.
18 (*a*) R. Shapiro, *Mutagen*, 1977, **39**, 149–175; (*b*) D. Zhang, X. Wang, X. Tian, L. Zhang, G. Yang, Y. Tao, C. Liang, K. Li, X. Yu, X. Tang, *et al.*, *Front. Immunol.*, 2018, **9**, 00882.
19 H. F. Jin, Y. Wang, X. B. Wang, Y. Sun, C. S. Tang and J. B. Du, *Nitric Oxide*, 2013, **32**, 56–61.